nature structural & molecular biology

The evolutionary capacitor HSP90 buffers the regulatory effects of mammalian endogenous retroviruses

Barbara Hummel[1,2], Erik C Hansen[1], Aneliya Yoveva[1,2], Fernando Aprile-Garcia[1], Rebecca Hussong[1] & Ritwick Sawarkar[1]

Understanding how genotypes are linked to phenotypes is important in biomedical and evolutionary studies. The chaperone heat-shock protein 90 (HSP90) buffers genetic variation by stabilizing proteins with variant sequences, thereby uncoupling phenotypes from genotypes. Here we report an unexpected role of HSP90 in buffering *cis*-regulatory variation affecting gene expression. By using the tripartite-motif-containing 28 (TRIM28; also known as KAP1)-mediated epigenetic pathway, HSP90 represses the regulatory influence of endogenous retroviruses (ERVs) on neighboring genes that are critical for mouse development. Our data based on natural variations in the mouse genome show that genes respond to HSP90 inhibition in a manner dependent on their genomic location with regard to strain-specific ERV-insertion sites. The evolutionary-capacitor function of HSP90 may thus have facilitated the exaptation of ERVs as key modifiers of gene expression and morphological diversification. Our findings add a new regulatory layer through which HSP90 uncouples phenotypic outcomes from individual genotypes.

Diversification of form and function during evolution is driven by changes in *cis*-regulatory sequences in numerous cases[1]. Natural selection acts on preexisting genetic variation in promoter and enhancer regions, thereby rewiring transcriptional networks during speciation. Recent studies have indeed documented substantial variation in regulatory sequences in natural populations of flies compared with humans[2,3]. However, under normal conditions, only little gene-expression variation and minor phenotypic differences are present within a population. Developmental programs are thought to be 'buffered' or 'canalized' to produce very similar phenotypes despite genetic variation[4]. One possible molecular example of such buffering ability involves the chaperone HSP90, which stabilizes key proteins in signaling pathways and transcriptional networks. HSP90 is thought to facilitate the accumulation of genetic variation in a population without having large consequences on an individual's reproductive fitness. Decreased HSP90 function leads to phenotypic manifestation of cryptic genetic variation in budding yeast, *Drosophila*, *Arabidopsis* and natural populations of fish[5–8]. Thus, HSP90 has been proposed to function as an evolutionary capacitor allowing natural populations to accumulate genetic variation, and this genetic variation is potentially released as phenotypic variation under stressful conditions that compromise HSP90 function[9].

Despite the broad ramifications of the buffering ability of HSP90, surprisingly little is known about the molecular basis of this function. HSP90-buffered traits in yeast have been mapped to protein-coding as well as *cis*-regulatory regions of the genome[5]. Although protein variants can be buffered by HSP90 via their stabilization, it is not clear how the chaperone minimizes the transcriptional effects of regulatory variation in promoter and enhancer sequences. Recent work has shown that HSP90 binds chromatin at gene regulatory elements in flies and mammals and stabilizes transcriptional and epigenetic factors, thus possibly explaining the buffering of regulatory variation[10–13]. Advances in population genomics and large-scale efforts to functionally annotate promoters and enhancers have provided a framework in which to investigate HSP90-mediated buffering of *cis*-regulatory variation.

Natural insertions of transposable elements (TEs) in regulatory regions present a rich source of variation within a population. Indeed genome sequencing of 18 distinct mouse strains has uncovered abundant variation in TE insertions across the genome[14]. TEs are transcriptionally repressed by epigenetic mechanisms including trimethylation of histone H3 at Lys9 (forming H3K9me3) and DNA methylation[15]. TEs in the germline are additionally silenced by post-transcriptional piwi-interacting RNA (piRNA) mechanisms that depend on HSP90 (refs. 16–18). In *Drosophila*, depletion of HSP90 function in germ cells causes transposition of TEs to new genomic positions, thereby possibly disrupting critical genes[19]. Rather than buffering preexisting genetic variation, the germline-specific function of HSP90 controls *de novo* variation, thus leading to heritable phenotypic diversity[19].

In somatic cells, even without transposition, TEs influence the expression of nearby genes and consequently organismal phenotypes, as exemplified by a TE insertion near the agouti locus in mice[20]. The gene-regulatory potential of TEs has also fueled evolutionary diversification and innovation in craniofacial development and mammalian pregnancy[21–23]. It is unclear how randomly integrated TEs initially appearing as genetic variations within a population ultimately regulate the expression of critical genes and thus developmental trajectories. We sought to determine whether the evolutionary capacitor HSP90

[1]Max Planck Institute of Immunobiology and Epigenetics, Freiburg, Germany. [2]Faculty of Biology, University of Freiburg, Freiburg, Germany. Correspondence should be addressed to R.S. (sawarkar@ie-freiburg.mpg.de).

Received 12 July 2016; accepted 22 December 2016; published online 30 January 2017; doi:10.1038/nsmb.3368

might facilitate fixation of mouse TEs in a population by first buffering the consequences of new TE insertions in the few individuals that carry these variations.

RESULTS

If HSP90 buffers genetic variation caused by TE insertions in gene-regulatory regions and thus acts as an evolutionary capacitor, two testable predictions can be made. First, HSP90 would control TE expression and its effect on nearby host genes in somatic cells, thereby mitigating the developmental and phenotypic effects associated with TE insertions. Second, individuals in natural populations would accumulate genetic variation caused by TEs without exhibiting any overt differences in gene-expression profiles, as long as HSP90 is functional. In the present study, we tested these predictions by using gene-expression signature as a quantitative phenotype contingent on TE-induced genetic variation.

HSP90 and the repression of ERVs in somatic cells

To test whether HSP90 regulates the transcription of TEs in somatic cells, we selected three distinct cell types from mice representing different developmental stages and lineages: pluripotent embryonic stem cells (ESCs), multipotent neuronal progenitor cells (NPCs) and bone-marrow-derived macrophages as primary differentiated cells. The cells were treated with nanomolar concentrations of NVP-AUY922, a specific and potent small-molecule inhibitor of HSP90 (Online Methods and ref. 24). Use of this pharmacological inhibition rather than genetic or RNA-interference-mediated depletion of HSP90 protein allowed us to expose cells to mild modulation of the chaperone activity over a short term, thereby avoiding effects on cell viability and compensatory expression of the two HSP90 isoforms (**Supplementary Table 1** and **Supplementary Fig. 1a**). NVP-AUY922 is currently being used in clinical trials as an anticancer therapeutic and has been proven to be a highly specific HSP90 inhibitor[25].

The global changes in the transcriptomes of all three cell types as a result of HSP90 inhibition were assessed by RNA sequencing (RNA-seq) in triplicate. To determine whether HSP90 inhibition affects the transcriptional activity of TEs, we mapped the RNA-seq reads to the mouse genome. Unexpectedly, a fraction of TEs were significantly up- or downregulated after HSP90 inhibition (**Fig. 1a–e**, **Supplementary Fig. 1b–g** and **Supplementary Table 2**). Of the approximately 1,400 types of repetitive elements analyzed, 175, 88 and 144 types were upregulated in ESCs, NPCs and macrophages, respectively (with a fold change greater than two and an adjusted P value <0.01, on the basis of DESeq2 analysis of three independent cell cultures, as outlined in Online Methods; **Supplementary Fig. 1g**). Genome-browser views of normalized data from RNA-seq confirmed the analysis (**Fig. 1d**,**e** and **Supplementary Fig. 1b–f**). TEs such as intracisternal A particle type Ez (IAPEz) were upregulated in all three cell types, whereas other subtypes exemplified by mouse ERV type L (MERV-L) were affected in a cell-type-specific manner (**Supplementary Table 2**). We validated our observations by using an independent method of reverse transcription followed by quantitative PCR (RT–qPCR; **Fig. 1f**). In addition, we observed the increases in IAPEz and MERV-L at two lower concentrations of HSP90 inhibitor without inducing a heat-shock response (**Supplementary Fig. 1h**). The robust changes in the repertoire of TE expression supported the possibility that HSP90 regulates TEs in the examined cell types representing various developmental lineages.

Mammalian TEs can be classified into two broad groups—DNA transposons and retrotransposons—depending on the requirement of an RNA intermediate for the transposition reaction. Retrotransposons can be further subdivided into long or short interspersed nuclear elements (LINEs and SINEs, respectively) and long terminal repeat (LTR) transposons[26]. The sequences within the LTR transposons can be traced back to mammalian retroviruses that probably resulted from primary infection of viruses in the germline[27]. The LTR transposons are thus termed ERVs. The various classes of TEs are silenced through distinct epigenetic pathways. Hence, misregulation of any particular type of TEs would reflect compromised specific molecular mechanisms. An overwhelming majority of TEs misregulated after HSP90 inhibition in all three cell types belonged to the class of ERVs (**Fig. 1g** and **Supplementary Table 2**), thus implicating HSP90 in specific pathways regulating TEs in the mouse genome. In this study, to dissect the capacitor function of HSP90, we focused on ERVs that were upregulated after HSP90 inhibition.

Genes neighboring ERVs are upregulated by HSP90 inhibition

Only a small number of mammalian ERVs are intact and capable of transposing to a new location[28]. Even if they integrate at ectopic sites in the genome after HSP90 inhibition, such *de novo* variation in somatic cells is not heritable and hence is of little evolutionary consequence. Transcriptionally activated ERVs may instead influence regulation of host genes in the vicinity of preexisting insertion sites and consequently affect phenotypes after HSP90 inhibition. We tested whether the capacitor function of HSP90 buffers or minimizes regulatory effects of ERVs on host genes within 200 kb of the ERV insertions annotated in the mouse genome. Indeed, host genes located within 25 kb up- or downstream of preexisting ERV-insertion sites were upregulated in cells with compromised HSP90 activity (**Fig. 2a**, **Supplementary Fig. 2a** and **Supplementary Table 3**). Importantly, the effect on the neighboring genes was restricted to ERVs targeted by HSP90 for silencing: MERV-L and IAPEz in ESCs (**Fig. 2a**) and IAPEz in NPCs (**Supplementary Fig. 2a**). A closely related ERV, origin-region repeat 1 type D2 (ORR1D2), which was not misregulated after HSP90 inhibition, did not show any consistent effect on genes in its vicinity. Thus, under normal conditions, the chaperone activity of HSP90 minimizes the regulatory influence of ERVs on neighboring genes.

To dissect the neighborhood effect further, we focused on genes that were immediate neighbors of the ERVs not farther than 25 kb away, because the effect on gene expression was consistent only within this range (**Fig. 2a**). On average, genes next to IAPEz, as compared with all expressed genes in the genome, showed an increase in expression after HSP90 inhibition, irrespective of the cell type examined (**Fig. 2b** and **Supplementary Fig. 2b**). In agreement with MERV-L being induced by HSP90 inhibition only in ESCs, immediate neighboring genes of MERV-L were upregulated in ESCs, but there were no significant changes in their expression in NPCs and macrophages (**Fig. 2c**). As expected, adjacent genes located beyond 25 kb from their closest ERV, as compared with adjacent genes within 25 kb, showed a decreased effect after HSP90 inhibition (**Supplementary Fig. 2b–f**).

ERVs are known to regulate nearby genes in some cases by forming a chimeric transcript originating from the LTR region and continuing through the adjacent gene. Using the paired-end RNA-seq data, we found that HSP90 inhibition increased chimeric transcription of several genes close to MERV-L and IAPEz, but not ORR1D2 (**Supplementary Table 4**). We independently confirmed the enhanced chimeric transcription of three genes after HSP90 inhibition by using PCR and gel electrophoresis as well as RT–qPCR (**Fig. 2d** and **Supplementary Fig. 2g–k**). The cell-type-specific neighborhood effect and chimeric transcription induced by HSP90 inhibition suggested

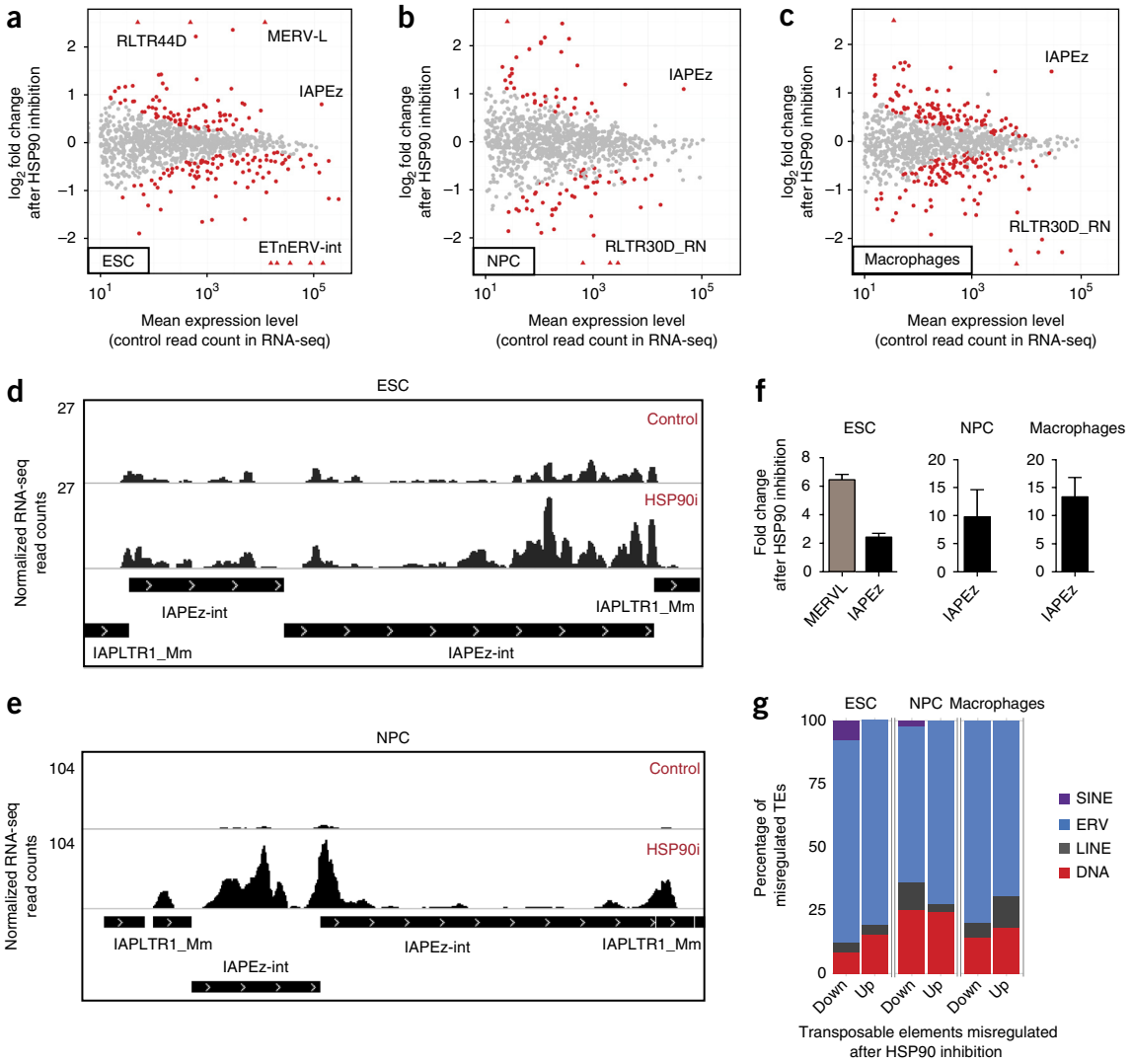

Figure 1 HSP90 inhibition causes misregulation of TEs in different mouse cell types. (**a**–**c**) Changes in expression of all annotated TEs after HSP90 inhibition in ESCs (**a**), NPCs (**b**) and macrophages (**c**), plotted against the mean expression levels under control conditions. Data obtained by RNA-seq analysis are shown as means from 3 independent cell cultures. TEs with significant misregulation are highlighted in red (adjusted *P* value <0.01, on the basis of DESeq2 analysis of three independent cell cultures, as outlined in Online Methods). The list of all misregulated TEs with corresponding fold changes is available in **Supplementary Table 2**. (**d**,**e**) Genome-browser snapshot of genomic loci with indicated ERVs. RNA-seq read counts in control and HSP90 inhibition (HSP90i) conditions are plotted on the *y* axis. Genomic coordinates (mouse genome build mm10) are as follows: chromosome 7, 137894161–137901058 (**d**) and chromosome 10, 59381391–59388056 (**e**). (**f**) RT–qPCR analyses of a selected set of differentially expressed ERVs in the indicated cell types. Fold change is shown as mean and s.e.m. from two independent cell cultures. (**g**) The proportion of different TE subtypes up- or downregulated after HSP90 inhibition in the indicated cell types.

that ERV upregulation is causally associated with increased expression of neighboring genes rather than being a direct effect of HSP90 inhibition on genes themselves. Thus, transcription of mouse genes appears to become responsive to HSP90 inhibition depending on the genes' proximity to ERVs.

HSP90 cooperates with TRIM28 (KAP1) in restricting gene expression

ERV-adjacent genes that became ectopically activated after HSP90 inhibition typically showed a highly restricted expression pattern across mouse tissues (**Fig. 3a** and **Supplementary Fig. 3a**,**b**). Many of the ectopically expressed genes perform essential tasks in development and physiology (**Fig. 3b** and **Supplementary Fig. 3c**,**d**), thus emphasizing the potential phenotypic effects of their misregulation. HSP90 probably keeps the ability of ERVs to rewire the host transcriptional network in check by repressing the ERVs, thereby maintaining phenotypic robustness. Compromise in the chaperone activity of HSP90 is thus likely to alter the developmental trajectory or physiological function of differentiated cells.

It is unclear how HSP90 regulates the expression of ERVs, thereby restricting tissue-specific gene expression. As a molecular chaperone, HSP90 might stabilize clients, such as transcription factors and chromatin regulators, that are involved in the epigenetic repression of ERVs. Deletion or knockdown of such a client protein would be expected to cause an ERV upregulation similar to that seen in HSP90 inhibition. We used published RNA-seq data sets from ESCs with depletion of proteins required for TE repression, such as histone deacetylases; histone methyltransferases (G9a, SET-domain bifurcated 1 (SETDB1) and suppressor of variegation 3-9h (SUV39h)); and co-repressors (heterochromatin protein 1 (HP1) and tripartite

motif-containing 28 (TRIM28, hereafter referred to as KAP1 for Krüppel-associated box–associated protein 1))[29–37]. Hierarchical clustering of data sets on the basis of changes in expression of ERVs resulted in a tree grouping HSP90 together with KAP1 and SETDB1 (**Fig. 3c**). The KAP1 co-repressor recruits the H3K9 methyltransferase SETDB1 to ERVs[38], and the clustering of SETDB1 and KAP1 together with HSP90 implicates the chaperone in this epigenetic-repression pathway. Various independent lines of evidence further confirmed that KAP1 and HSP90 cooperatively repress ERVs. First, genes upregulated in *Kap1* (official symbol *Trim28*)- and *Setdb1*-knockout cells significantly overlapped with those in HSP90-inhibited ESCs (**Fig. 3d** and **Supplementary Table 3**). A detailed analysis of the extent of overlap revealed a much larger set of genes co-regulated by HSP90 and KAP1 as compared with HSP90 and SETDB1 (**Supplementary Fig. 4a**). This observation raises the possibility that HSP90 may chaperone KAP1 not only in the context of SETDB1 but also in KAP1 complexes with other chromatin regulators or transcription factors[25]. Second, genes neighboring MERV-L and IAPEz were upregulated after *Kap1* knockout in a manner quantitatively similar to that observed after HSP90 inhibition (comparison of **Fig. 2a** with **Supplementary Fig. 4b**). Individual ERV-gene pairs known to be regulated by KAP1-dependent H3K9me3 were also upregulated after HSP90 inhibition (**Supplementary Fig. 5**). In agreement with previously reported results[30], *Setdb1* knockout showed an effect only on genes neighboring IAPEz, but not MERV-L (**Supplementary Fig. 4c**). In the case of both *Setdb1*- and *Kap1*-knockout cells, genes close to ORR1D2 were not affected, similarly to the effects in HSP90 inhibited ESCs. Third, we identified chimeric transcripts that were induced to a similar extent under both HSP90-inhibition and *Kap1*-knockout conditions, as exemplified by Rimklb, starting from an MT2B2 LTR region (**Supplementary Fig. 4d** and **Supplementary Table 4**). Fourth, HSP90 and KAP1 interacted with each other, as shown by reciprocal immunoprecipitations (**Fig. 3e**,**f**). These data from mouse ESCs corroborate independently reported interactions between HSP90 and KAP1 in the human cancer cell line K562, identified in an unbiased manner[39]. Finally upregulation of MERV-L and IAPEz after HSP90 inhibition requires functional KAP1, because KAP1-deficient ESCs[40] showed an attenuated increase in ERVs in response to HSP90 inhibition (**Fig. 3g**).

How might HSP90 regulate ERVs via the KAP1 pathway? KAP1 stability does not depend on HSP90 function (**Fig. 3h**, inset), as might be suspected from the direct chaperoning of KAP1 by HSP90. Nonetheless, HSP90 colocalized with KAP1 at the tested ERVs (**Supplementary Fig. 6a**), and KAP1 binding to chromatin required HSP90 activity (**Fig. 3h** and **Supplementary Fig. 6b**). Given that the repressive H3K9me3 mark at IAPEz was dependent on KAP1 (**Supplementary Fig. 6c**,**d**), we analyzed whether this chromatin modification was also affected after HSP90 inhibition. The loss of chromatin-bound KAP1 at IAPEz after HSP90 inhibition was accompanied by a decrease in H3K9me3 at this region (**Fig. 3h** and **Supplementary Fig. 6b**), thus confirming that KAP1-mediated recruitment of repressive machinery to ERVs requires HSP90 activity. The depletion of this repressive histone modification in HSP90 inhibitor-treated ESCs was not a result of a global effect, because Suvar39h-dependent H3K9 trimethylation[31] at major satellites was not significantly affected by the treatment (**Fig. 3h**). Thus, through a combination of computational, biochemical and genetic approaches, our data support a model in which HSP90 and KAP1 cooperatively mediate ERV repression in ESCs.

HSP90 buffers strain variations due to ERV insertions

ERVs have the potential to affect the expression of genes located near their insertion sites. Because the ERV-insertion sites are variable across

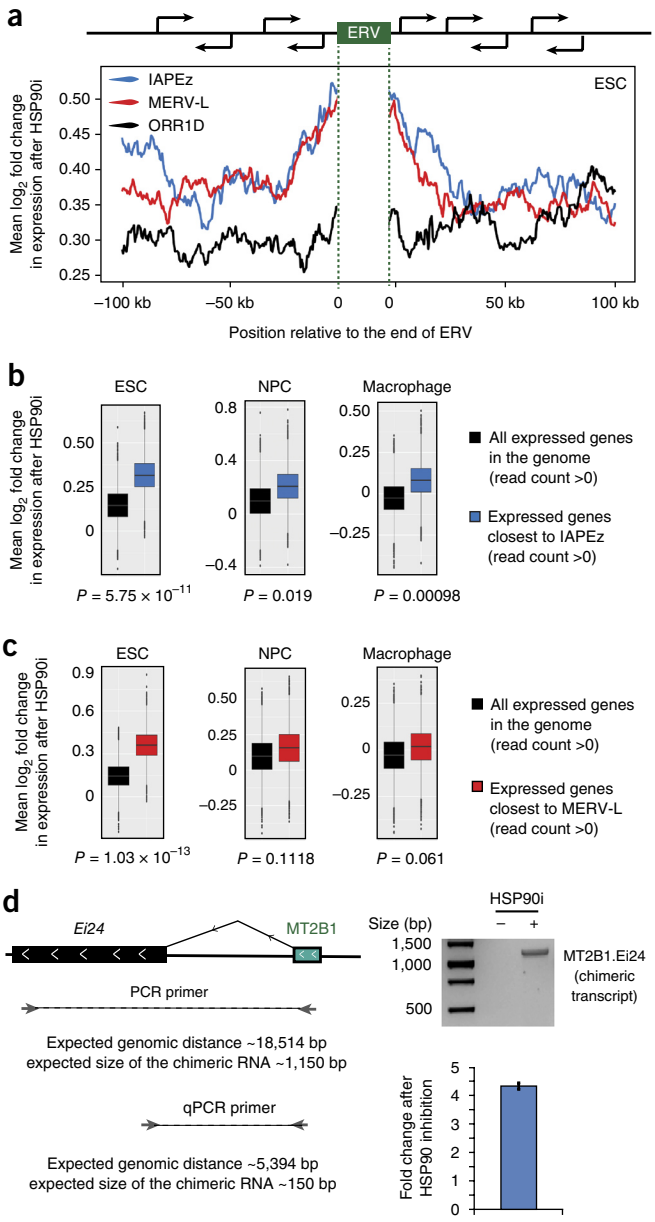

Figure 2 HSP90 inhibition affects expression of genes in the vicinity of ERVs. (**a**) HSP90-inhibition-induced changes in the expression of genes located within a 200-kb region around ERV insertions in ESCs. The analyzed subtypes of ERVs are shown in different colors. (**b**,**c**) HSP90-inhibition-induced changes in expression of all transcribed genes in the genome (black boxes), in comparison with expressed genes adjacent to IAPEz (blue boxes in **b**) and MERV-L (red boxes in **c**). Only adjacent genes within 25 kb from the ERV were considered. Box plots display the 25th to 75th percentiles (boxes), medians (lines) and 1.5× the interquartile range (whiskers). Outliers are depicted as individual dots. *P* values calculated by two-sided Wilcoxon rank-sum test (based on RNA-seq of three independent cell cultures) are shown below each comparison and denote the significance of the difference between the corresponding sets of genes. (**d**) Top left, schematic showing the chimeric transcript starting from the MT2B1 LTR region and continuing to the neighboring gene *Ei24*. Top right, agarose gel showing an RT–PCR product of 1,150 bp, expected only in the presence of transcriptional fusion and splicing, in samples treated with HSP90 inhibitor. Bottom, RT–qPCR analyses using the indicated primer pair (schematics at left) showed a large increase in the amount of chimeric transcript after Hsp90 inhibition (bar graph at right, mean ± s.e.m. from 3 independent cell cultures).

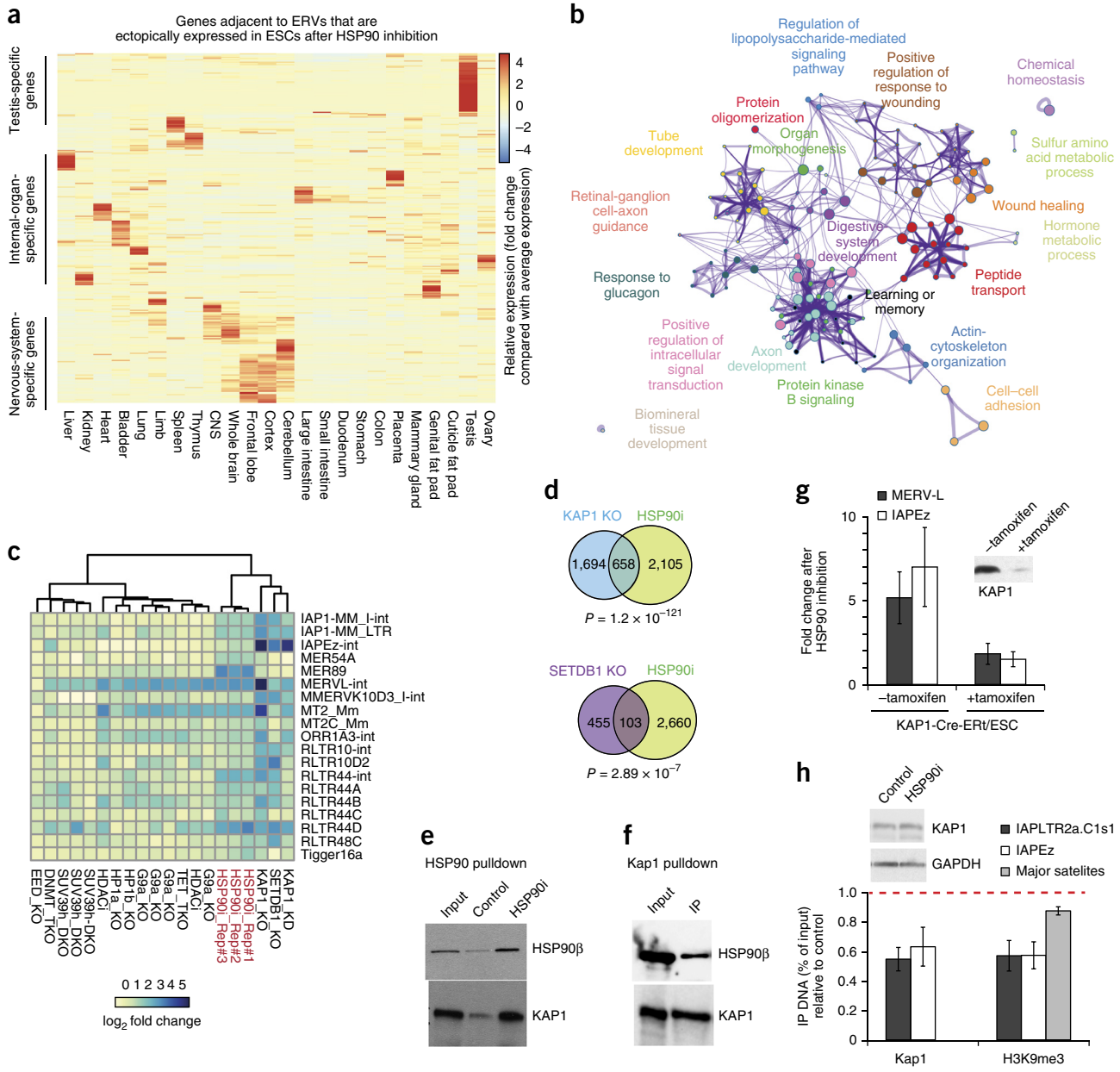

Figure 3 HSP90 represses cell-type-specific genes and ERVs through the KAP1–SETDB1 pathway. (**a**) Heat map showing the expression of selected genes across indicated mouse tissues or cell types. Genes adjacent to ERVs that are ectopically expressed in ESCs after HSP90 inhibition were selected for this analysis. The heat map was generated with RNA-seq data from ENCODE. (**b**) Genes in **a**, clustered on the basis of common gene-ontology terms, as indicated. (**c**) Hierarchical clustering of RNA-seq data on the basis of fold changes in ERV expression after HSP90 inhibition (reported here) and depletion of the specified chromatin regulators (data from published sources; details in Online Methods). KO, knockout; DKO, double knockout; TKO, triple knockout; KD, knockdown. (**d**) Venn diagrams depicting the overlap of genes upregulated in ESCs with knockout of either *Kap1* (top) or *Setdb1* (bottom), as compared with genes upregulated after HSP90 inhibition. *P* values were calculated with a hypergeometric test and show the significance of the overlap. (**e**) Western blots showing the presence of HSP90 and KAP1 proteins in complexes enriched by using immobilized HSP90 inhibitor (HSP90i) or an inactive drug (control). (**f**) Western blots showing the presence of HSP90 and KAP1 proteins in complexes enriched by using antibody against KAP1. IP, immunoprecipitation. (**g**) RT–qPCR analyses showing the effect of HSP90 inhibition on the expression of the indicated ERVs, in *Kap1* wild-type ESCs (–tamoxifen) and *Kap1*-knockout ESCs (+tamoxifen). Fold changes are shown as mean ± s.e.m. from three independent cell cultures. Inset, KAP1 immunoblot demonstrating *Kap1* knockout induced by tamoxifen treatment of floxed *Kap1* cells. (**h**) Chromatin IP–qPCR for KAP1 and H3K9me3 in ESCs treated with or without HSP90 inhibitor. Enrichment relative to control conditions is shown as mean ± s.e.m. of three independent cell cultures. Red dotted line indicates enrichment signal in the control condition. Inset, KAP1 immunoblot showing that KAP1 stability is unchanged after HSP90 inhibition.

individuals, owing to random ancestral transposition events, distinct sets of genes are likely to exhibit ERV-mediated misregulation in different individuals. By repressing ERVs with the help of KAP1, HSP90 may minimize the transcriptional consequences of ERV insertions and hence buffer the corresponding genetic variation in a population.

We tested this important tenet of the buffering hypothesis in two models of genetic variation by using either synthetically altered ERV-insertion sites or naturally available polymorphisms in the mouse genome.

To experimentally modify the existent ERV insertions, we focused on an instance of IAPLTR2 integrated approximately 3.5 kb upstream

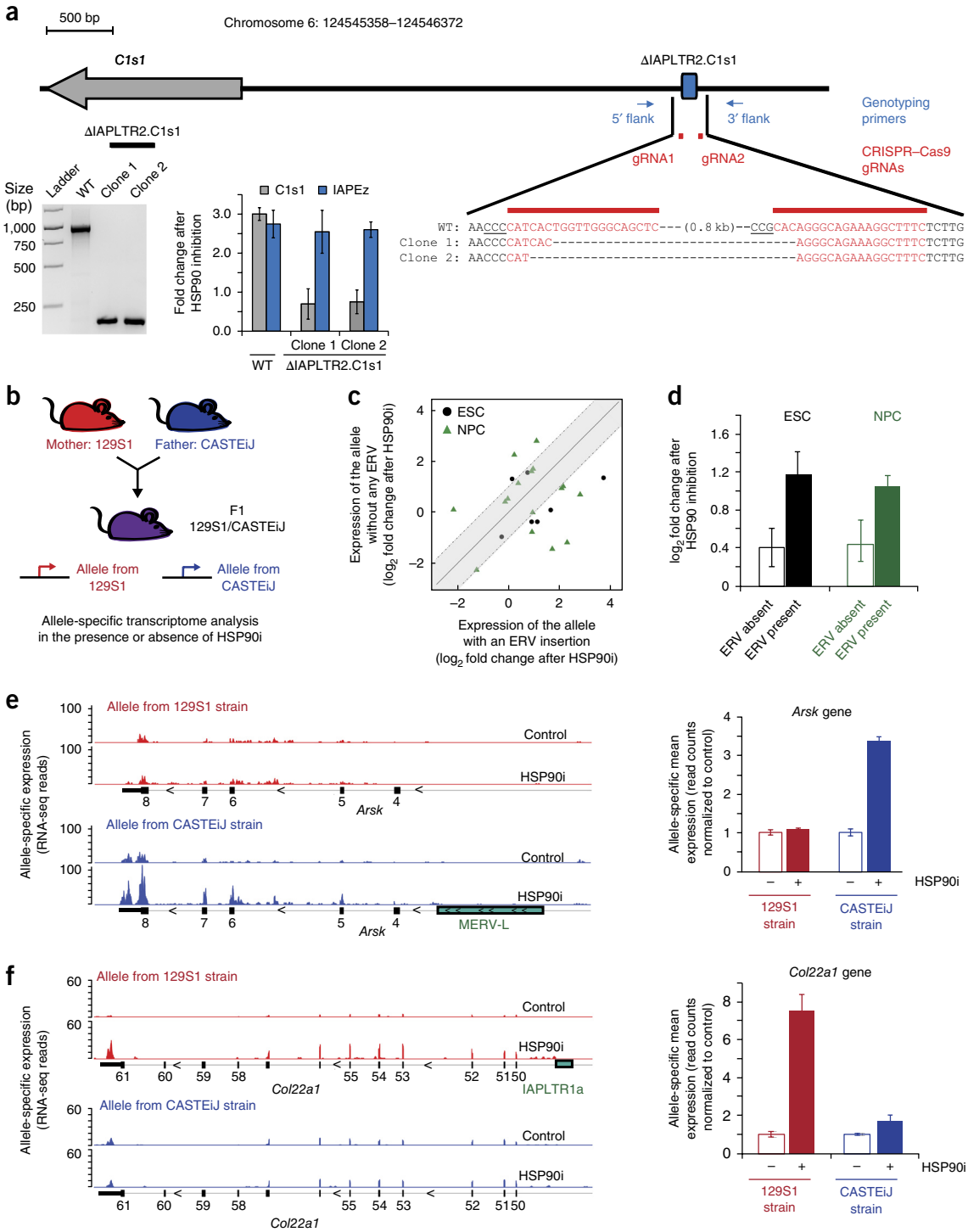

Figure 4 Genetic variation caused by preexisting ERV insertions is buffered by HSP90. (**a**) Top, schematic of genotyping primers and guide RNAs (gRNAs) used for the design and validation of CRISPR–Cas9-mediated deletion of IAPLTR2 upstream of the *C1s1* gene. Bottom left, agarose gel genotyping two independent clones to confirm deletion of IAPLTR2. Bottom right, bar graph showing the effect of HSP90 inhibition on expression of IAPEz and *C1s1*, as determined by RT–qPCR in both clones; data are shown as mean ± s.e.m. from 3 independent cell cultures for each clone. (**b**) Experimental design to study the effect of HSP90 inhibition on allele-specific expression of genes. (**c**) Allele-specific changes in expression after HSP90 inhibition. Alleles neighboring either MERV-L or IAPEz insertion are plotted on the *x* axis. Alleles without either MERV-L or IAPEz insertion in proximity are plotted on the *y* axis. Black circles, expression changes in ESCs; green triangles, expression changes in NPCs. (**d**) HSP90-inhibition-induced changes in the expression of alleles from the two parental strains, grouped according to the presence or absence of nearby MERV-L or IAPEz in ESCs (black) and NPCs (green). The *y* axis shows average expression (mean ± s.e.m.) of seven genes for ESC and 16 genes in NPC. (**e**,**f**) Genome-browser profiles of unprocessed RNA-seq reads at the *Arsk* locus in ESCs (**e**) and at the *Col22a1* locus in NPCs (**f**). Only reads that mapped to one of the two alleles are plotted. At the *Arsk* locus, MERV-L is inserted in the CASTEiJ strain, whereas at the *Col22a1* locus IAPLTR1a is inserted in the 129S1 strain, as shown. The strain-specific effects of HSP90 inhibition on the expression of the two genes, as assessed by RNA-seq, are plotted on the right as mean ± s.e.m. from three independent cell cultures.

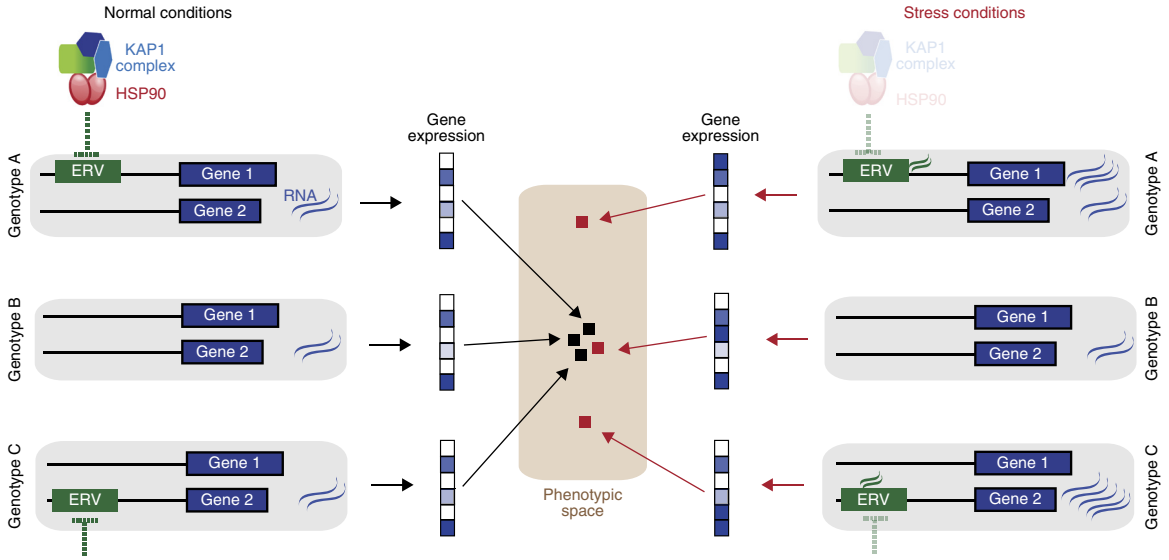

Figure 5 The role of HSP90 and stress in genotype–phenotype mapping through buffering gene-expression variation caused by ERVs. A model showing three genetic variants (A, B and C) with different locations of ERV in their genomes (denoted by two genes). The HSP90–KAP1 complex buffers the regulatory effects of ERV on host genes, thus resulting in similar gene-expression patterns and phenotypes among the three variants. Stress conditions cause a compromise in the buffering ability of HSP90, thus activating the target ERVs and nearby host genes, which are distinct in each individual. Thus, the three genetic variants have different gene-expression patterns after stress or HSP90 inhibition, and possibly have divergent phenotypic outcomes.

of the gene *C1s1* in the genome (a region referred to as *C1s1.IAPLTR2*). This LTR region showed KAP1 and an H3K9me3 signal that decreased after HSP90 inhibition (**Fig. 3h**), with a concomitant increase in expression of *C1s1* (**Supplementary Table 3**). We used the CRISPR–Cas9 system to delete *C1s1.IAPLTR2*, thus generating two independent clones isogenic with parental ESCs but lacking this particular instance of the ERV (**Fig. 4a**). After HSP90 inhibition, the two deletion clones showed an upregulation of IAPEz (from all instances of IAPEz insertions across the genome) comparable to that in the isogenic parental ESC, but did not activate *C1s1* expression (**Fig. 4a**). The removal of ERV from the neighborhood made the *C1s1* gene nonresponsive to HSP90 inhibition, thus strongly supporting the notion that insertion of ERVs makes nearby genes responsive to HSP90 inhibition.

We further tested the buffering ability of HSP90 by leveraging natural genetic variation in ERV-insertion sites. Comprehensive sequencing and annotation of whole genomes of several mouse strains allowed us to identify genes with strain-specific ERV insertions in the neighborhood (ref. 14 and **Supplementary Fig. 6e**). ESCs derived from 129S1 and CASTEiJ backgrounds carrying ERV insertions close to five genes were compared with ESCs derived from a C57BL6 background that did not have ERV insertions near these five genes. After HSP90 inhibition, all five genes were upregulated in 129S1-CASTEiJ ESCs but not in C57BL6 ESCs (**Supplementary Fig. 6e**), thus suggesting that natural variation in ERV-insertion sites may play an important role in responsiveness to HSP90 inhibition.

ESCs from two different genetic backgrounds exhibited differences in genomes beyond these five genes, thus providing a potential theoretical explanation for the differential responsiveness to HSP90 inhibition. To further refine this experiment with natural genetic variation, we used cells from F1 heterozygous offspring of two inbred strains, 129S1 and CASTEiJ. The maternal and paternal alleles, representing two individual mouse strains, shared an identical set of *trans*-acting factors in the cells of the F1 offspring (**Fig. 4b**). We investigated the correlation between strain-specific ERV insertions and changes in expression of the nearest gene after HSP90 inhibition. Allele-specific RNA-seq analysis in ESCs and NPCs derived from F1 heterozygotes confirmed that the allele with a nearby ERV, compared with the other allele of the same gene without any ERV, was significantly upregulated after HSP90 inhibition (**Fig. 4c–f**). For example, the *Arsk* gene from the CASTEiJ strain has an intronic MERV-L and was upregulated threefold after HSP90 inhibition (**Fig. 4e**). In comparison, the *Arsk* gene from the 129S1 strain has no ERV insertions nearby and showed little transcriptional change when HSP90 activity was decreased. Thus our genome-wide data based on natural genetic variation as well as targeted synthetic variation of one ERV instance confirm that the location of ERV insertions plays a crucial role in determining the transcriptional response of mouse genes to HSP90 inhibition.

Stress decreases the repressive effect of HSP90 on ERV

HSP90 function is compromised under various natural stresses, such as alterations in temperature, pH, salinity and toxicity of food[41]. To demonstrate that HSP90 inhibition mimics the effect of environmental factors, we exposed cells to stresses mimicking natural conditions such as fever temperatures, heavy-metal arsenic treatment and oxidative stress. All three stresses led to an upregulation of both MERV-L and IAPEz elements in ESCs, as shown by RT–qPCR (**Supplementary Fig. 6f**). Host genes near ERV-insertion sites are hence likely to respond to environmental stress similarly to their response to HSP90 inhibition.

In summary, the data presented here support a model in which HSP90 silences the transcriptional influence of ERVs on neighboring genes, in cooperation with KAP1. Genes near ERV-insertion sites in the sequenced mouse genomes encode proteins driving morphogenesis (**Fig. 3a,b**), thus making developmental trajectories responsive to stress in an HSP90-contingent manner. However, given the polymorphisms in ERV insertions within a population[42], distinct genes respond to the same stress in different individuals (**Fig. 5**). Thus, the differential transcriptional response of these genes after stress among members of a population is likely to lead to phenotypic variation, as shown in numerous studies[5–9,43]. In conclusion, our study indicates another mechanism by which HSP90 acts globally to buffer genetic variation in *cis*-regulatory regions.

DISCUSSION

By defining ERVs as one of the sources of HSP90-buffered genetic variation, our work paves the way for confirming important predictions of the evolutionary capacitor hypothesis. Linking of HSP90 with the epigenetic-repression machinery consequently connects the transcription of ERV to nearby genes after environmental stresses. The enormous number of ERV insertions in the mouse genome[15] suggests the possibility of an accumulation of genetic variation buffered by the capacitor HSP90. Most importantly, ERVs have driven transcriptional networks underlying major evolutionary innovations such as innate immune responses[44]. By allowing nearby genes to respond to pathogenic stimuli, ERVs have played an important role in the evolution of host defense and the expansion of ecological niches. HSP90 may have helped ERVs accumulate during evolutionary periods near genes, thus eventually making them responsive to external stimuli. By chaperoning transcriptional regulators, HSP90 has expanded its repertoire of buffered genetic variation from protein-coding regions to gene-regulatory noncoding elements.

Earlier studies in flies and mice have indicated the role of HSP90 in controlling transposition of TEs in the germline via piRNA pathways[18,45]. HSP90 mutants thus have a mutator phenotype, because transposition in the germline introduces new heritable genetic variation. Our studies support an additional, and perhaps unrelated, mechanism by which HSP90 shapes the role of TEs in evolution. First, the upregulation of genes neighboring ERVs, as reported here, is unlikely to be due to new transposition events, because we assessed only preexisting ERV locations annotated in the sequenced genomes. Second, HSP90-mutant germ cells exhibit a derepression of the LINE L1 element[45], which was transcriptionally unaffected in our experiments performed on somatic cells (**Supplementary Table 2**). Third, the transcriptional changes after HSP90 inhibition reported in this study were inferred from a population of cells, thus nullifying the effects of random transposition occurring in a minority of cells, if at all. Fourth, piRNA-based repression mechanisms have not been reported to operate in any of the cell types examined in this study. Moreover, recent reports have uncoupled the piRNA-dependent phenotypic effects of HSP90 mutations from transposition[46]. It appears that, in addition to repressing transpositions, HSP90 plays a critical role in neutralizing the transcriptional effects of preexisting TEs. Coordination of mutator and capacitor activities within the same chaperone system directed toward TEs makes HSP90 a more efficient facilitator of diversification than has previously been thought.

HSP90 is a specialized chaperone that also aids in the assembly of several multiprotein complexes. At the molecular level, HSP90 may facilitate the formation of the KAP1–SETDB1 co-repressor complex, either in the nucleoplasm or at chromatin. Alternatively, HSP90 may be required for the enzymatic activity of SETDB1 histone methyltransferase, which is required to repress ERVs. Given that HSP90 inhibition affects a smaller subset of KAP1- and SETDB1-regulated TEs in ESCs, it is more likely that HSP90 is needed for stabilization of a few transcription factors that recruit KAP1–SETDB1 to specific ERVs. Krüppel-associated-box zinc-finger proteins are known for their role in bringing the KAP1 co-repressor to chromatin[47], and some zinc-finger proteins have been found to interact with HSP90 in previous unbiased screens[48]. Additional transcription factors and chromatin regulators known to interact with HSP90 may also be involved[25]. A directed biochemical approach would be able to answer the specific molecular questions raised by our work.

Critical to the role of HSP90 as a buffer of regulatory variation described here is the rewiring of the transcriptional network by derepressed ERVs. Ectopic activation of tissue-specific genes with ontogenetic functions (**Fig. 3a**,**b** and **Supplementary Fig. 3**) may underlie the acquisition of new developmental or physiological functions. Reutilization of ancient genes in new tissue contexts is a recurrent evolutionary theme in the generation of new forms and functions[1]. For example, TE-driven placental expression of immune genes is thought to be important for maternal-fetal immunotolerance during the evolution of pregnancy[22]. Acquisition of new expression domains by key developmental genes may indeed be facilitated by the capacitor function of HSP90 via the KAP1–ERV axis described here. Thus, our studies provide a molecular framework in which to study HSP90's buffering function directed toward noncoding regulatory variation.

METHODS

Methods, including statements of data availability and any associated accession codes and references, are available in the online version of the paper.

Note: Any Supplementary Information and Source Data files are available in the online version of the paper.

ACKNOWLEDGMENTS

We thank A. Akhtar, U. Bönisch, T. Jenuwein, T. Lämmermann, T. Manke and E. Trompouki (Max Planck Institute of Immunobiology and Epigenetics) for valuable input, cells and reagents; and E. Heard (Institut Curie, France), D. Trono (EPFL), G. Chiosis (Memorial Sloan Kettering Cancer Center) and D. Schübeler (FMI) for kindly providing cells and reagents. We are grateful to R. Rebollo for insightful discussions. This work was financially supported by the Max Planck Society, German Research Foundation (DFG) through the collaborative research center 'Medical Epigenetics' and the Ambizione grant from the Swiss National Foundation (R.S.).

AUTHOR CONTRIBUTIONS

R.S. conceived the project; B.H. and R.S. designed the study; all authors performed experiments and interpreted the results; B.H. and R.S. wrote the manuscript with input from all authors.

COMPETING FINANCIAL INTERESTS

The authors declare no competing financial interests.

1. Wray, G.A. The evolutionary significance of *cis*-regulatory mutations. *Nat. Rev. Genet.* **8**, 206–216 (2007).
2. Mackay, T.F.C. *et al.* The *Drosophila melanogaster* Genetic Reference Panel. *Nature* **482**, 173–178 (2012).
3. Kilpinen, H. *et al.* Coordinated effects of sequence variation on DNA binding, chromatin structure, and transcription. *Science* **342**, 744–747 (2013).
4. Waddington, C. Canalization of development and the inheritance of acquired characters. *Nature* **150**, 563–656 (1942).
5. Jarosz, D.F. & Lindquist, S. Hsp90 and environmental stress transform the adaptive value of natural genetic variation. *Science* **330**, 1820–1824 (2010).
6. Queitsch, C., Sangster, T.A. & Lindquist, S. Hsp90 as a capacitor of phenotypic variation. *Nature* **417**, 618–624 (2002).
7. Rutherford, S.L. & Lindquist, S. Hsp90 as a capacitor for morphological evolution. *Nature* **396**, 336–342 (1998).
8. Rohner, N. *et al.* Cryptic variation in morphological evolution: HSP90 as a capacitor for loss of eyes in cavefish. *Science* **342**, 1372–1375 (2013).
9. Jarosz, D.F., Taipale, M. & Lindquist, S. Protein homeostasis and the phenotypic manifestation of genetic diversity: principles and mechanisms. *Annu. Rev. Genet.* **44**, 189–216 (2010).
10. Sawarkar, R., Sievers, C. & Paro, R. Hsp90 globally targets paused RNA polymerase to regulate gene expression in response to environmental stimuli. *Cell* **149**, 807–818 (2012).
11. Greer, C.B. *et al.* Histone deacetylases positively regulate transcription through the elongation machinery. *Cell Rep.* **13**, 1444–1455 (2015).
12. Sawarkar, R. & Paro, R. Hsp90@chromatin.nucleus: an emerging hub of a networker. *Trends Cell Biol.* **23**, 193–201 (2013).
13. Sollars, V. *et al.* Evidence for an epigenetic mechanism by which Hsp90 acts as a capacitor for morphological evolution. *Nat. Genet.* **33**, 70–74 (2003).
14. Nellåker, C. *et al.* The genomic landscape shaped by selection on transposable elements across 18 mouse strains. *Genome Biol.* **13**, R45 (2012).
15. Friedli, M. & Trono, D. The developmental control of transposable elements and the evolution of higher species. *Annu. Rev. Cell Dev. Biol.* **31**, 429–451 (2015).

16. Weick, E.M. & Miska, E.A. piRNAs: from biogenesis to function. *Development* **141**, 3458–3471 (2014).
17. Xiol, J. *et al.* A role for Fkbp6 and the chaperone machinery in piRNA amplification and transposon silencing. *Mol. Cell* **47**, 970–979 (2012).
18. Olivieri, D., Senti, K.A., Subramanian, S., Sachidanandam, R. & Brennecke, J. The cochaperone shutdown defines a group of biogenesis factors essential for all piRNA populations in *Drosophila*. *Mol. Cell* **47**, 954–969 (2012).
19. Specchia, V. *et al.* Hsp90 prevents phenotypic variation by suppressing the mutagenic activity of transposons. *Nature* **463**, 662–665 (2010).
20. Dolinoy, D.C. The agouti mouse model: an epigenetic biosensor for nutritional and environmental alterations on the fetal epigenome. *Nutr. Rev.* **66** (Suppl. 1), S7–S11 (2008).
21. Gifford, W.D., Pfaff, S.L. & Macfarlan, T.S. Transposable elements as genetic regulatory substrates in early development. *Trends Cell Biol.* **23**, 218–226 (2013).
22. Lynch, V.J. *et al.* Ancient transposable elements transformed the uterine regulatory landscape and transcriptome during the evolution of mammalian pregnancy. *Cell Rep.* **10**, 551–561 (2015).
23. Prescott, S.L. *et al.* Enhancer divergence and cis-regulatory evolution in the human and chimp neural crest. *Cell* **163**, 68–83 (2015).
24. Eccles, S.A. *et al.* NVP-AUY922: a novel heat shock protein 90 inhibitor active against xenograft tumor growth, angiogenesis, and metastasis. *Cancer Res.* **68**, 2850–2860 (2008).
25. Trepel, J., Mollapour, M., Giaccone, G. & Neckers, L. Targeting the dynamic HSP90 complex in cancer. *Nat. Rev. Cancer* **10**, 537–549 (2010).
26. Rebollo, R., Romanish, M.T. & Mager, D.L. Transposable elements: an abundant and natural source of regulatory sequences for host genes. *Annu. Rev. Genet.* **46**, 21–42 (2012).
27. Dewannieux, M. & Heidmann, T. Endogenous retroviruses: acquisition, amplification and taming of genome invaders. *Curr. Opin. Virol.* **3**, 646–656 (2013).
28. Faulkner, G.J. Retrotransposons: mobile and mutagenic from conception to death. *FEBS Lett.* **585**, 1589–1594 (2011).
29. Ferrari, K.J. *et al.* Polycomb-dependent H3K27me1 and H3K27me2 regulate active transcription and enhancer fidelity. *Mol. Cell* **53**, 49–62 (2014).
30. Karimi, M.M. *et al.* DNA methylation and SETDB1/H3K9me3 regulate predominantly distinct sets of genes, retroelements, and chimeric transcripts in mESCs. *Cell Stem Cell* **8**, 676–687 (2011).
31. Bulut-Karslioglu, A. *et al.* Suv39h-dependent H3K9me3 marks intact retrotransposons and silences LINE elements in mouse embryonic stem cells. *Mol. Cell* **55**, 277–290 (2014).
32. Franci, G. *et al.* The class I-specific HDAC inhibitor MS-275 modulates the differentiation potential of mouse embryonic stem cells. *Biol. Open* **2**, 1070–1077 (2013).
33. Maksakova, I.A. *et al.* Distinct roles of KAP1, HP1 and G9a/GLP in silencing of the two-cell-specific retrotransposon MERVL in mouse ES cells. *Epigenetics Chromatin* **6**, 15 (2013).
34. Mozzetta, C. *et al.* The histone H3 lysine 9 methyltransferases G9a and GLP regulate polycomb repressive complex 2-mediated gene silencing. *Mol. Cell* **53**, 277–289 (2014).
35. Macfarlan, T.S. *et al.* Embryonic stem cell potency fluctuates with endogenous retrovirus activity. *Nature* **487**, 57–63 (2012).
36. Rowe, H.M. *et al.* TRIM28 repression of retrotransposon-based enhancers is necessary to preserve transcriptional dynamics in embryonic stem cells. *Genome Res.* **23**, 452–461 (2013).
37. Lu, F. *et al.* Role of Tet proteins in enhancer activity and telomere elongation. *Genes Dev.* **28**, 2103–2119 (2014).
38. Schultz, D.C., Ayyanathan, K., Negorev, D., Maul, G.G. & Rauscher, F.J. III. SETDB1: a novel KAP-1-associated histone H3, lysine 9-specific methyltransferase that contributes to HP1-mediated silencing of euchromatic genes by KRAB zinc-finger proteins. *Genes Dev.* **16**, 919–932 (2002).
39. Moulick, K. *et al.* Affinity-based proteomics reveal cancer-specific networks coordinated by Hsp90. *Nat. Chem. Biol.* **7**, 818–826 (2011).
40. Rowe, H.M. *et al.* KAP1 controls endogenous retroviruses in embryonic stem cells. *Nature* **463**, 237–240 (2010).
41. Sangster, T.A., Lindquist, S. & Queitsch, C. Under cover: causes, effects and implications of Hsp90-mediated genetic capacitance. *BioEssays* **26**, 348–362 (2004).
42. Zhang, Y., Maksakova, I.A., Gagnier, L., van de Lagemaat, L.N. & Mager, D.L. Genome-wide assessments reveal extremely high levels of polymorphism of two active families of mouse endogenous retroviral elements. *PLoS Genet.* **4**, e1000007 (2008).
43. Sangster, T.A. *et al.* HSP90-buffered genetic variation is common in *Arabidopsis thaliana*. *Proc. Natl. Acad. Sci. USA* **105**, 2969–2974 (2008).
44. Chuong, E.B., Elde, N.C. & Feschotte, C. Regulatory evolution of innate immunity through co-option of endogenous retroviruses. *Science* **351**, 1083–1087 (2016).
45. Ichiyanagi, T. *et al.* HSP90α plays an important role in piRNA biogenesis and retrotransposon repression in mouse. *Nucleic Acids Res.* **42**, 11903–11911 (2014).
46. Gangaraju, V.K. *et al. Drosophila* Piwi functions in Hsp90-mediated suppression of phenotypic variation. *Nat. Genet.* **43**, 153–158 (2011).
47. Iyengar, S. & Farnham, P.J. KAP1 protein: an enigmatic master regulator of the genome. *J. Biol. Chem.* **286**, 26267–26276 (2011).
48. Taipale, M. *et al.* Quantitative analysis of HSP90-client interactions reveals principles of substrate recognition. *Cell* **150**, 987–1001 (2012).

ONLINE METHODS

Cell culture, inhibitor treatment, RNA extraction and processing. ESCs (obtained from E Heard) were grown in 2i (two-inhibitor) medium with standard protocols for maintenance and passaging. NPCs (obtained from A. Akhtar) were cultured as described previously[49]. Macrophages were derived from bone marrow of 4-month-old female mice with a BALBc/C57BL6 background (a kind gift from T. Lämmermann) by using recombinant murine macrophage colony stimulating factor (M-CSF; PeproTech, cat. no. 315-02) according to standard protocols. Animal experiments were done in accordance with German animal protection law (paragraph 4, section 3). Genotypes of cells in culture were confirmed by analyzing RNA-seq data. Cells were tested for mycoplasma contamination with PCR. ESCs and NPCs shared the same genetic background because they were derived from an offspring of the cross between a 129S1 female and a CASTEiJ male.

The HSP90 inhibitor NVP-AUY922 was purchased from LC Laboratories. The optimal concentration of NVP-AUY922 was empirically determined for each cell line used, such that no effect on cell viability was observed after 24 h. HSP90 inhibition experiments on macrophages were performed between the seventh and eighth days after cells were collected from mouse bone marrow. HSP90 inhibition was carried out with the following concentrations of NVP-AUY922 for 16 h with the corresponding cell types: 100 nM for ESCs, 500 nM for macrophages and 50 nM for NPCs. We confirmed a lack of cytotoxicity in the RNA-seq data (**Supplementary Table 1**). In addition, we performed experiments in ESCs with 50 nM and 75 nM NVP-AUY922 for 16 h to expose cells to nonproteotoxic conditions (shown in **Supplementary Figs. 1h** and **6e**). To mimic natural stressful conditions, we exposed ESCs to fever temperatures (39.5 °C), As_2O_3 (final concentration 100 nM) and H_2O_2 (final concentration 5 μM) for 16 h.

After treatment, cells were resuspended in peqGOLD Trifast (VWR International, cat. no. 30-2010), and RNA was extracted according to the manufacturer's protocol. DNase I treatment was carried out for 2 h to eliminate genomic DNA contamination, by using a TURBO DNase kit (Thermo Fisher Scientific, cat. no. AM1907). RNA was analyzed either with RT–qPCR or paired-end poly(A) RNA sequencing with an Illumina HiSeq system.

For RT–qPCR, reverse transcription was performed with random primers and a first-strand cDNA synthesis kit (Thermo Fisher, cat. no. K1612). Absolute SYBR Green Rox mix (Thermo Scientific, cat. no. AB1163) was used for qPCR, which was carried out on an Applied Biosystems StepOne Plus instrument. Data were quantified with the ΔΔCt method and were normalized to GAPDH expression. For agarose gel analysis, cDNA input was normalized before PCR amplification, and products were run on a 2% agarose gel.

RNA-seq data were analyzed for the occurrence of chimeric transcripts, as described in ref. 31. Three chimeric transcripts were evaluated by qPCR and PCR with primers spanning the junction site of the ERV LTR region and the adjacent gene. Primers were designed with Primer3 software (http://frodo.wi.mit.edu/). All primer sequences used in this study are shown in **Supplementary Table 5**.

Computational analyses of RNA-seq data. RNA-seq reads were trimmed with TrimGalore (v0.4.0; http://www.bioinformatics.babraham.ac.uk/projects/trim_galore/) and mapped to Ensembl annotation release 78 with TopHat2 (v2.0.13; ref. 50) with the options mate-inner-dist, mate-std-dev and library-type (fr-firststrand). The distances between read mates (mate-inner-dist and mate-std-dev) were assessed individually with RSeQC (v2.6.1; ref. 51). After mapping of the RNA-seq reads from all samples to the mouse genome build mm10, the reads that mapped uniquely to the genome were counted with featureCounts[52] with the following options: --Q 10 --p --B --C --s 2. The annotations present in the *Mus musculus* gtf file from Ensembl release 78 were used as a reference for counting. DESeq2 (ref. 53) was used for differential expression analysis. Genes with an adjusted *P* value <0.01 were defined as significantly affected. Raw reads were downloaded from publicly available RNA-seq data (Kap1, GSE74278; Setdb1 and Dnmt, GSE29413) and processed as described above.

In addition, RNA-seq reads from ESCs, NPCs and macrophages were analyzed in an allele-specific manner through methodology described in a recent study[54]. Briefly, two pseudogenomes were generated for both parental genotypes with known SNPs and indels from the Mouse Genomes Project (downloaded from ftp://ftp-mouse.sanger.ac.uk/REL-1410-SNPs_Indels/). Reads were mapped to maternal and paternal pseudogenomes. Both alignments were then merged to define the origin of a read (maternal genome, paternal genome or indistinguishable). Allele-specific expression changes were calculated with a generalized linear model within DESeq2 (ref. 53).

Allele-specific expression was correlated with known polymorphic ERVs with data from a recent study[13]. Only ERVs that were present and annotated in the reference strain (C57Bl6), were considered. ERVs present in 129S1 or CASTEiJ, but not in the reference C57Bl6 strain, had no subclassification (such as IAPEz, MERV-L) and therefore could not be used for the analysis. Of the ERV instances present in only one of the two parental strains (129S1 and CASTEiJ), we used those belonging either to MERV-L or IAPEz. ERV-gene pairs were then shortlisted only if the gene had at least one SNP in its exonic region to distinguish the two alleles. Because we were interested in ERV insertions responsible for inducing expression of nearby genes, we filtered out all genes that did not exhibit significantly changed allele-specific expression patterns. Additionally, we observed that genes that were induced after HSP90i were more weakly expressed than genes that remained unchanged or were downregulated after inhibition. Therefore, we removed the top 25% highly expressed genes.

For tissue-specific gene-expression plots, RPKM values from ENCODE data (http://promoter.bx.psu.edu/ENCODE/downloads/mm65.long.gene.with.expr.cshl.tsv) were clustered and visualized with the 'pheatmap' package[55].

Analysis of repetitive elements. RNA-seq reads were mapped to the mouse genome assembly mm10 with Bowtie2 (ref. 56) with random assignment of multimapping reads. Reads with more than three mismatches were discarded. RepeatMasker annotations (downloaded from the UCSC genome browser on 28 July 2015) were used as input for the bamCoverage subcommand of the BEDtools suite[57] to count repetitive-element reads with the --split option. Differential expression was analyzed with DESeq2 (ref. 53).

To investigate the factor mimicking the effect of HSP90 inhibition, we used publicly available RNA-seq data sets in the presence or absence of known ERV repressors. Raw reads were downloaded from publicly available RNA-seq data (EED, GSE51006; DNMT, GSE29413; SUV39h, GSE57092; HDAC, GSE45909; HP1, GSE47370; G9a, GSE46545 and GSE36896; Kap1, GSE41903; Setdb1, GSE29413; and TET, GSE56986) (refs. 30–38) and processed as described above. Hierarchical clustering was limited to ERV elements that were upregulated after HSP90 inhibition with at least 100 reads. Visualization was done with the pheatmap function available in the pheatmap[55] R package with the Euclidean distance metric and ward agglomeration method.

Neighborhood analysis. To analyze the expression changes of genes in the flanking regions of ERVs, we merged elements of the same type within 400 bp. The 100-kb flanking regions on both sides were then binned with the flank and window subcommands in the BEDtools suite[57]. Genes overlapping those bins were identified with the intersectBed subcommand. Custom scripts were used to combine all genes within the same bin of each type of ERV element. Within each bin, a gene was considered only once. All genes, for which a $\log_2$ fold change could not be determined by DESeq2 (ref. 53), owing to numerical problems, were removed from the analysis. Calculation and plotting of the mean $\log_2$ fold change of all genes per bin was done with a custom R script with the ggplot2 package[58].

To further define the neighborhood effect, we next considered only the closest up- and downstream gene with the closestBed subcommand of the BEDtools suite[57]. Again, only genes for which a $\log_2$ fold change could be determined by DESeq2 were considered. Genes adjacent to more than one ERV (IAPEz, MERV-L or ORR1D2) were removed from the analysis to decrease compound effects. We performed two-sided Wilcoxon tests to investigate whether genes closer to certain ERV elements, as compared with all genes, showed a higher upregulation on average after HSP90 inhibition.

For plot design, we applied a random subsampling approach. To obtain a distribution of $\log_2$ fold changes that could be expected by chance, we subsampled the set of all genes with at least one RNA-seq read count with a sample size of 100 and calculated the mean $\log_2$ fold change for each subset of genes (total number of considered annotated transcribed regions: 21,753 (ESC); 18,212 (NPCs) and 17,294 (macrophages)). This step was repeated 10,000 times. To compare the $\log_2$ fold changes of all genes with those of the genes closest to ERVs (**Supplementary Fig. 2b**), the same subsampling approach was also applied to the set of closest up- and downstream genes for each ERV instance in the genome. Both distributions are plotted as box plots with the ggplot2 package[58].

ChIP–seq and ChIP–qPCR analysis. For publicly available data, raw reads were downloaded for H3K9me3 (GSE41903) and KAP1 (GSE58323) ChIP–seq experiments and trimmed with TrimGalore (v0.4.0; http://www.bioinformatics.babraham.ac.uk/projects/trim_galore/). Mapping was done with Bowtie2 with default parameters and mouse genome build mm10. Bigwig files and profile plots were generated with the bamCoverage, computeMatrix and plotProfile modules of the deepTools package[59]. Peaks were called by using MACS2 (ref. 60).

KAP1 and H3K9me3 ChIP were performed under standard conditions as previously described[61], with anti-KAP1 (Abcam, ab22553) and anti-H3K9me3 (a kind gift from T. Jenuwein)[31]. HSP90 ChIP was performed on ESCs expressing biotin-tagged HSP90 that were generated as previously described[62], with a modified chromatin preparation protocol from ref. 61. ChIP DNA was purified with phenol–chloroform extraction and ethanol precipitation and used for ChIP–qPCR. Enrichment of the immunoprecipitated DNA at the corresponding loci was expressed as a percentage relative to the input DNA.

Pulldown, knockdown and knockout experiments. HSP90 and KAP1 complexes were purified from ESC extracts with PU-H71 beads, as previously described[40], or with anti-KAP1 (Abcam, ab22553), respectively. The enriched complexes were blotted and probed with anti-HSP90β (Abcam, ab53497) or anti-KAP1 (Abcam, ab22553). Antibody validation is provided on the manufacturer's website. Antibody validation is provided on the manufacturer's website. HSP90 isoforms were knocked down with shRNA as previously described[63], with suggestions from C. Miething (University Clinic Freiburg). Conditional knockout of KAP1 was generated with floxed KAP1 cells (gift from D. Trono), according to a previously published protocol[37].

Generation and analysis of IAPEz deletion with CRISPR–Cas9. Guide RNA (gRNA) sequences were designed to generate a specific deletion of IAPEz upstream of the *C1s1* gene with 'Chopchop' (https://chopchop.rc.fas.harvard.edu/). Each gRNA sequence was verified to be a unique target in the mouse genome with BLAT and was tested for efficiency with T7 endonuclease assays[64]. gRNA oligonucleotides were cloned into pSpCas9(BB)-2A-EGFP or pSpCas9(BB)-2A-Puro vectors. pSpCas9(BB)-2A-GFP (PX458) and pSpCas9(BB)-2A-PURO (PX459) V2.0 were a gift from F. Zhang (Addgene plasmid nos. 48138 and 62988, respectively).

Mouse ESCs grown on feeder cells were cotransfected with both gRNA constructs and were either FACS-sorted (EGFP) or placed under puromycin (1 μg/mL) selection for 3 d. Clonal cell lines were established with limiting dilution cloning. Clones were screened for homozygous deletions by using PCR with flanking primer pairs at the expected genomic deletion site (**Fig. 4a**). Deletion sequences were confirmed through direct sequencing of PCR products with Sanger sequencing.

Data availability. All the sequencing data generated in this study have been deposited in the Gene Expression Omnibus database under accession number GSE87119. Other data are available from the corresponding author after reasonable request.

49. Chelmicki, T. *et al.* MOF-associated complexes ensure stem cell identity and Xist repression. *eLife* **3**, e02024 (2014).
50. Kim, D. *et al.* TopHat2: accurate alignment of transcriptomes in the presence of insertions, deletions and gene fusions. *Genome Biol.* **14**, R36 (2013).
51. Wang, L., Wang, S. & Li, W. RSeQC: quality control of RNA-seq experiments. *Bioinformatics* **28**, 2184–2185 (2012).
52. Liao, Y., Smyth, G.K. & Shi, W. featureCounts: an efficient general purpose program for assigning sequence reads to genomic features. *Bioinformatics* **30**, 923–930 (2014).
53. Love, M.I., Huber, W. & Anders, S. Moderated estimation of fold change and dispersion for RNAseq data with DESeq2. *Genome Biol.* **15**, 550 (2014).
54. Huang, S., Holt, J., Kao, C.Y., McMillan, L. & Wang, W. A novel multi-alignment pipeline for high-throughput sequencing data. *Database (Oxford)* **2014**, bau057 (2014).
55. Kolde, R. pheatmap: Pretty Heatmaps. R package v. 1.0.8. (2015).
56. Langmead, B. & Salzberg, S.L. Fast gapped-read alignment with Bowtie 2. *Nat. Methods* **9**, 357–359 (2012).
57. Quinlan, A.R. & Hall, I.M. BEDTools: a flexible suite of utilities for comparing genomic features. *Bioinformatics* **26**, 841–842 (2010).
58. Wickham, H. ggplot2: Elegant Graphics for Data Analysis. (Springer, 2009).
59. Ramírez, F. *et al.* deepTools2: a next generation web server for deep-sequencing data analysis. *Nucleic Acids Res.* **44**, W1, W160-5 (2016).
60. Zhang, Y. *et al.* Model-based analysis of ChIP-Seq (MACS). *Genome Biol.* **9**, R137 (2008).
61. Arrigoni, L. *et al.* Standardizing chromatin research: a simple and universal method for ChIP-seq. *Nucleic Acids Res.* **44**, e67 (2016).
62. Baubec, T., Ivánek, R., Lienert, F. & Schübeler, D. Methylation-dependent and -independent genomic targeting principles of the MBD protein family. *Cell* **153**, 480–492 (2013).
63. Dow, L.E. *et al.* A pipeline for the generation of shRNA transgenic mice. *Nat. Protoc.* **7**, 374–393 (2012).
64. Ran, F.A. *et al.* Genome engineering using the CRISPR-Cas9 system. *Nat. Protoc.* **8**, 2281–2308 (2013).